

AUS Repository

Synthesis of Metal-Organic Framework from Iron Nitrate and 2,6-Naphthalenedicarboxylic Acid and Its Application as Drug Carrier

Item Type	Peer-Reviewed;Article;Published version
Authors	Ibrahim, Mihad;Sabouni, Rana;Husseini, Ghaleb
Citation	Ibrahim, M., Sabouni, R., & Husseini, G. A. (2018). Synthesis of metal-organic framework from iron nitrate and 2,6-naphthalenedicarboxylic acid and its application as drug carrier. <i>Journal of Nanoscience and Nanotechnology</i> , 18(8), 5266–5273. https://doi.org/10.1166/jnn.2018.15373
DOI	10.1166/jnn.2018.15373
Publisher	American Scientific Publishers
Download date	2026-05-20 15:46:52
Link to Item	http://hdl.handle.net/11073/19731

Synthesis of Metal-Organic Framework from Iron Nitrate and 2,6-Naphthalenedicarboxylic Acid and Its Application as Drug Carrier

Mihad Ibrahim, Rana Sabouni, and Ghaleb A. Hussein*

Department of Chemical Engineering, American University of Sharjah, Sharjah, United Arab Emirates

Metal-organic frameworks (MOFs) are highly crystalline porous organic–inorganic materials that are comprised of metal salts and organic linkers. The common synthetic methodologies of MOFs include: solvothermal, microwave-assisted, electrochemical, mechanochemical, and sonochemical routes. The synthesized MOF particles can be characterized using several characterization techniques including: X-ray diffraction (XRD), scanning electron microscopy (SEM), Fourier transform infrared spectroscopy (FTIR), and other analytical techniques. Recently, MOFs have garnered increasing attention due to their potential applications in numerous areas including: catalysis, gas storage and separation, drug delivery, and others. In this research paper, a new metal-organic framework was synthesized successfully from iron nitrate and 2,6-naphthalenedicarboxylic acid (1) by means of microwave irradiation (Fe-NDC-M) and (2) solvothermally using a conventional electric oven (Fe-NDC-O). They were characterized using XRD, SEM, FTIR, energy-dispersive X-ray (EDS), and thermogravimetric analysis (TGA). The characterization results showed that the synthesized samples were crystals with a rod-like shape and particle sizes in the nanometer range. As a result, the new Fe-NDC-MOF particles can be used as nanocarriers for drug delivery applications utilizing the enhanced permeability and retention effect.

Keywords: Metal-Organic Frameworks, Solvothermal, Microwave-Assisted, XRD, SEM, FTIR, EDS, TGA, N₂ Sorption Experiments, Drug Delivery.

1. INTRODUCTION

Recently, metal-organic frameworks (MOFs) have been intensively researched as a new innovative class of porous coordination complexes. They are defined as hybrid solid organic–inorganic networks that essentially consist of metal salts (clusters) coordinated to organic compounds (ligands) to form one-, two-, or three-dimensional assemblies.^{1–4} MOFs are highly crystalline polymers with extensive surface areas and high porosity.^{5–7} Their Brunauer-Emmett-Teller (BET) surface area can reach up to ~7000 m²/g.^{8,9}

There are several routes used to synthesize MOFs, generally by combining the metal clusters with the organic ligands under controlled conditions. These routes include but are not limited to solvothermal, microwave, electrochemical, mechanochemical, and sonochemical procedures. Conventional solvothermal, and microwave assisted syntheses are the common routes used.^{7,10}

The conventional solvothermal reaction is the standard methodology of preparing MOFs, in which the reactants are heated in the presence of polar solvents (e.g., *N,N*-dimethylformamide, *N,N*-diethylformamide, methanol, and ethanol) in a closed vessel. When water is used as the solvent, the process is called hydrothermal synthesis.^{3,7,11} The main advantages of this methodology are (1) its simplicity and (2) the ability to control the morphology of the synthesized crystalline particles.^{11,12} Several MOFs have been synthesized solvothermally including: MOF-5, MOF-74, and MOF-177.¹²

Metal-organic frameworks (MOFs) can also be prepared using the microwave-assisted route, which relies on the interaction between electromagnetic waves and mobile electric charges (polar solvent and reactants). It is a promising technique that is used to obtain smaller MOF crystals with a controlled particle size distribution in a short time by heating of the reactants uniformly.^{3,13–15} Despite the advantages of this synthetic approach, the lack

*Author to whom correspondence should be addressed.

and difficulty of finding the morphological data of the resulting particles, which usually have very small sizes (in nanometers), limit its use.^{3,16,17} Examples of MOFs synthesized using this procedure include MOF-5, ZIF-8, and IRMOF-3.¹⁰

After preparing the MOFs (using metal salts and organic compounds) via one of the synthesis methods discussed above, the resulting particles can be characterized analytically via X-ray diffraction (XRD), scanning electron microscopy (SEM), energy-dispersive X-ray (EDS), and Fourier transform infrared spectroscopy (FTIR).¹⁸ Then, the characterized MOF crystals can be studied as drug delivery vehicles directly or after functionalization.

MOFs have generated considerable interest due to their tunable pore sizes, versatile functionality, and chemical and thermal stability.^{6,7,14,19} The flexibility in designing unlimited structures of MOFs with unique chemical and physical features renders them useful in a wide range of applications including: gas storage and separation (HKUST-1, IRMOF-6, and MOF-177),^{20,21} catalysis (MOF-5, IRMOF-3, and MIL-53),²² luminescence (Ln-MOFs and NMOF-1),²³ and other uses.^{3,6,7,24}

Biomedical engineering is one of the emerging areas that started utilizing MOFs. The porous nature of MOFs promotes favorable host-molecule interactions, and thus they can be used as nanovehicles for loading and delivering therapeutic agents to targeted areas in the body.^{25–27} The important properties required to use MOFs for drug delivery purposes are: low cytotoxicity, biocompatibility, the ability to carry high drug loadings with controlled release, and the ability to be detected by imaging techniques.^{5,28} In addition, the size of MOFs plays an important role, especially for *in vivo* applications. The particles should be in the nanometer range; so that they can circulate systematically in the blood.^{5,28,29}

Férey and co-workers investigated the first MOF family, namely MIL (MIL = Materials of Institut Lavoisier), investigated as “smart” drug nanocarriers; due to its large

pores (25–34 Å) and increased surface areas (3100–5900 m²/g).^{5,26} It is synthesized using trivalent metals (clusters) and carboxylic acid groups (linkers). In an attempt to reduce the side effects of some therapies, several successful drug delivery systems based on nontoxic porous Fe-MIL complexes were studied, including the encapsulation of Ibuprofen (anti-inflammatory drug) in MIL-100 and MIL-53, Cidofovir (retroviral drug) in MIL-89, MIL-88A, MIL-100, and MIL-53, and Azidothymidine triphosphate (retroviral drug) in MIL-88A, MIL-100, MIL-53, and MIL-101_NH₂. The particle sizes of MIL-89, MIL-88A, MIL-100, MIL-53, and MIL-101_NH₂ were found to be 50–100 nm, 150 nm (bimodal distribution of sizes, with micrometric particles), 200 nm, 350 nm (bimodal distribution of sizes, with micrometric particles), and 120 nm, respectively. All of these MOFs were prepared under solvothermal conditions or via microwave.^{5,28,29}

Several examples of MOF anticancer drug delivery systems were reported in literature including the loading of Ethoxysuccinato-cisplatin (ESCP) in functionalized Fe-MIL-101,³⁰ Doxorubicin in Fe-MIL-100, Busulfan in Fe-MIL-89, Fe-MIL-88A, Fe-MIL-100, and Fe-MIL-53,^{5,28,29} Camptothecin in 70-nm ZIF-8 nanoparticles³¹ and others. More recently, a new effective strategy based on capped MOFs was developed to enhance and control the release of the therapeutic agent by utilizing nanoMOFs gated by nanovalves including the incorporation of Doxorubicin in CP5-capped UMCM-1-NH-Py,³² 5-Fluorouracil in capped UiO-66-NH-Q and CP5-capped UiO-66-NH-A.^{33,34} The nanoparticles were prepared solvothermally, and the sizes of UMCM-1-NH-Py, UiO-66-NH-Q, and UiO-66-NH-A were calculated to be 332.1 ± 22 nm in water (decreased after the capping and loading), 100–200 nm, and 20 nm (increased to around 40 nm after capping and loading), respectively.^{32–34}

Numerous structures of MOFs based on 2,6-naphthalenedicarboxylic acid (2,6-NDC) as a ligand were reported. An example of a three-dimensional open

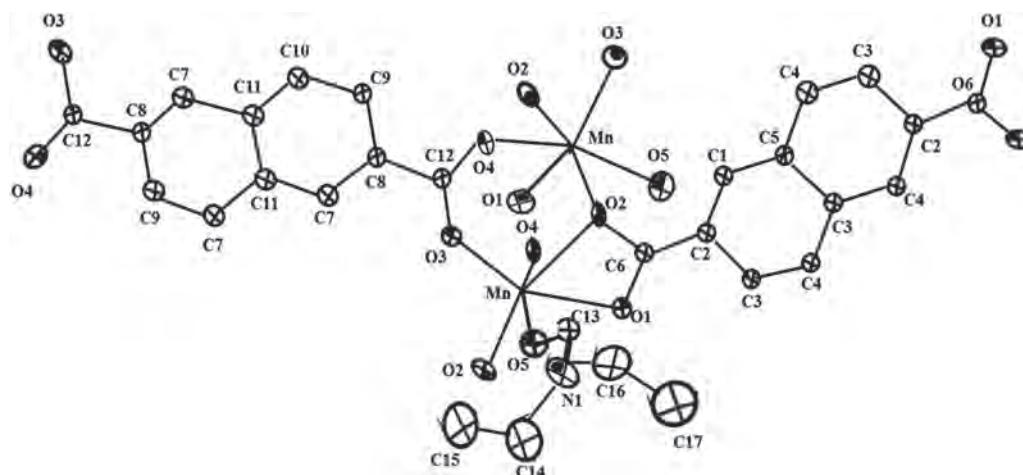


Figure 1. The ORTEP drawing of $[\text{Mn}(\text{NDC})(\text{DEF})]_n$.³⁵

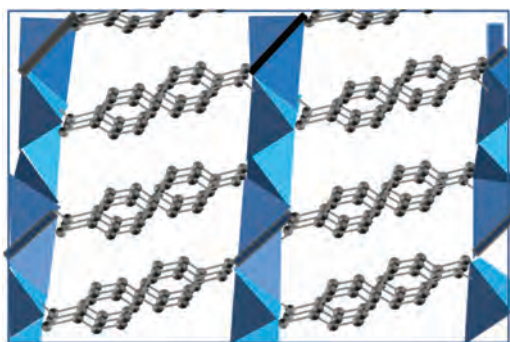


Figure 2. A view of $\text{Li}_2(2,6\text{-NDC})$ showing the connectivity of the organic layer with the antifluorite type LiO layer.³⁶

2,6-NDC-MOF architecture and its desolvated solid was described by Suh et al.³⁵ They synthesized the MOF under solvothermal conditions by heating a *N,N*-diethylformamide mixture of $\text{Mn}(\text{NO}_3)_2 \cdot n\text{H}_2\text{O}$ and 2,6-NDC at 105 °C for 24 h. The produced pale-yellowish crystals had a block shape with 1D channels. Figure 1 depicts the ORTEP drawing of $[\text{Mn}(\text{NDC})(\text{DEF})]_n$.

To obtain the desolvated MOF, the as-synthesized 2,6-NDC-MOF was heated in a Schlenk tube at 250 °C under vacuum for 18 h. Then later, desolvated MOF, had coordinatively unsaturated metal ion (Mn^{II}) sites. It was used to adsorb several gases, and the results showed that its adsorption capacities of N_2 , CO_2 , and CH_4 were higher than those of H_2 . On the other hand, its adsorption capacity of CO_2 was higher than that of CH_4 . Therefore, the desolvated 2,6-NDC-MOF can be used in the purification of H_2 as well as in the removal of CO_2 from the natural gas.³⁵

Parise et al. prepared another 2,6-NDC-MOF based on lithium as a metal cluster.³⁶ The synthesis was carried out by dissolving LiNO_3 , 2,6-NDC, and NH_4F in *N,N*-dimethylformamide. The resultant gel was stirred for 4 h and then heated at 180 °C for 5 days. Three-dimensional, yellowish needle crystals of $\text{Li}_2(2,6\text{-NDC})$ were obtained. The MOF structure contained a novel two-dimensional antifluorite layer of LiO connected by the organic linker (2,6-NDC) as shown in Figure 2.³⁶ Despite the rarity of lithium-based MOFs and their use, the $\text{Li}_2(2,6\text{-NDC})$ MOF can be used for hydrogen storage; as recent experiments

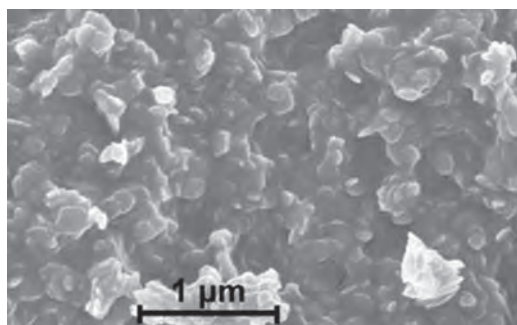


Figure 3. The SEM image of $\text{Al}(\text{OH})(\text{ndc})$.³⁸

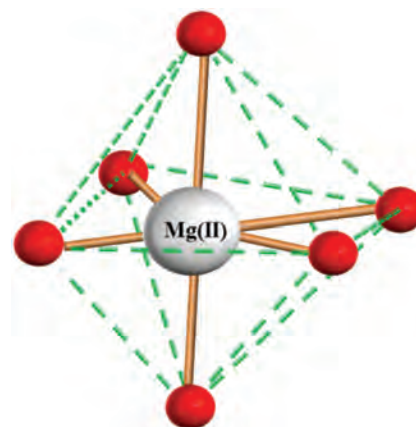


Figure 4. The coordination geometry of $[\text{Mg}_3(\text{NDC})_3(\text{DMF})_4] \cdot \text{H}_2\text{O}$.³⁹

indicated an incremental increase in H_2 uptake by MOF-5 when it was decorated with lithium.³⁷

In 2009, Senkovska et al. synthesized a highly porous MOF $[\text{Al}(\text{OH})(\text{ndc})]$. A typical synthesis procedure involved using a solvothermal reaction and thus heating a homogeneous solution of $\text{Al}(\text{NO}_3)_3 \cdot 9\text{H}_2\text{O}$ and 2,6-NDC dissolved in *N,N*-DMF at 120 °C for 24 h. Figure 3 represents the SEM image of $\text{Al}(\text{OH})(\text{ndc})$. The main problem of aluminium coordination MOFs is the difficulty in obtaining suitable single crystals.³⁸

Very recently, another three-dimensional 2,6-NDC-MOF structure was designed by Jonnalagadda and coworkers via the solvothermal route. It was prepared from $\text{MgCl}_2 \cdot 6\text{H}_2\text{O}$ and 2,6-NDC using *N,N*-DMF and water as solvents. The resultant solution was heated at 120 °C over three days, and white three-dimensional network crystalline particles were produced.³⁹

Figure 4 shows the coordination geometry of $[\text{Mg}_3(\text{NDC})_3(\text{DMF})_4] \cdot \text{H}_2\text{O}$, in which the central metal adopts a six-coordinated octahedral geometry. To use the synthesized MOF as a heterogeneous catalyst, coordinatively unsaturated Mg^{2+} centers can be created upon activation at temperatures ranging between 250 °C and 300 °C.

2. EXPERIMENTAL DETAILS

In this research paper, a new metal-organic framework was synthesized successfully from iron nitrate and 2,6-naphthalenedicarboxylic acid

(1) by means of microwave irradiation (Fe-NDC-M), and (2) solvothermally using a conventional electric oven (Fe-NDC-O).

To the best of the authors' knowledge, the Fe-NDC MOF was synthesized for the first time via two synthesis techniques using 2,6-NDC as the organic linker and iron nitrate as the metal cluster for drug delivery applications.

2.1. Selection of Building Blocks

The metal cluster (iron nitrate) was chosen since iron is naturally found in hemoglobin and is approximately

22 μM in the blood plasma.^{26,40} On the other hand, 2,6-naphthalenedicarboxylic acid was selected as the organic linker, because of its low toxicity.²⁵ However, *in vivo* and *in vitro* experiments should be conducted to determine the cytotoxicity of the prepared MOFs before their clinical use. Several parameters should be considered while synthesizing the MOFs for drug delivery applications, for future clinical use, such as: toxicity, particle size, stability, and pore volume.^{5, 26–28}

2.2. Synthesis

All starting chemicals were used as received from LABCO (the official Sigma-Aldrich distributor in the United Arab Emirates) without further purification. For comparison purposes, the MOFs were synthesized using two synthesis routes: (1) by means of microwave irradiation and (2) solvothermally using a conventional electric oven.

To synthesize the MOF using the microwave irradiation technique (Fe-NDC-M), typical amounts of 0.2307 mmol (93.2 mg) of iron(III) nitrate nonahydrate ($\text{Fe}(\text{NO}_3)_3 \cdot 9\text{H}_2\text{O}$, ACS reagent, $\geq 98\%$) and 0.2307 mmol (49.9 mg) of 2,6-naphthalenedicarboxylic acid (2,6-NDC, 99%) were dissolved in 10 mL of *N,N*-dimethylformamide (DMF, ReagentPlus[®], $\geq 99\%$). Then, the solution was poured in a 23-mL Teflon autoclave bomb calorimeter and heated in a microwave at 160 W for 5 min. To separate the produced particles (Fe-NDC-M), the resulting mixture was centrifuged at 5,500 rpm for 30 min. Then, the supernatant was removed, and the pale yellowish particles were washed twice with 5 mL of fresh DMF to remove the unreacted materials. Finally, the collected MOF particles were dried in an electric oven at 100 °C to evaporate all the DMF.

The same batch composition, as that utilized in the microwave technique (described above), was used to prepare the MOF using the conventional solvothermal method (Fe-NDC-O). The solution was heated in the oven (instead of a microwave) at 100 °C for 24 h. The remaining steps were carried out as described above.

2.3. Characterization Tests

To determine the morphological features of the synthesized samples, the nanoparticles were characterized using: X-ray diffraction (XRD), scanning electron microscopy (SEM), energy-dispersive X-ray (EDS), Fourier transform infrared spectroscopy (FTIR), and thermogravimetric analysis (TGA).

XRD data were recorded using a conventional high-resolution Bruker D8 Advance diffractometer using a Cu Ka ($k = 1.54 \text{ \AA}$) radiation source on a silicon wafer, from 3 to 40° (2θ) with a step size of 0.02° and 1 s (per step), in a continuous mode. The SEM (scanning electron microscope) images were obtained by MIRA3 XMU (Tescan Orsay Holding Company, Czech Republic). Prior to taking the SEM images, the MOFs samples were coated with gold to make them electrically conductive.

The EDS quantitative analysis for both MOFs was performed as follows: a small amount of the sample was placed in an aluminum stub inside a scanning electron microscope (VEGA III XMU with Oxford X-Max 50 EDS) and the results were collected using the Aztec software. Despite the limitation of EDS analysis in detecting light elements (such as hydrogen), it can still be used as a characterization technique.⁴¹

Spectrum one FT-IR spectrometer was used to obtain the IR spectra. First, tiny amounts of the MOFs were added to 200 mg of potassium bromide (FT-IR grade, $\geq 99\%$ trace metals basis from Sigma-Aldrich Company) and grinded manually. Then, the samples were compressed by applying 3,000 tons uniaxial pressure, and the resulting discs were placed inside the spectrometer. To test the thermal stability of the synthesized MOFs, the samples were analyzed using thermogravimetric analysis (TGA) Perkin Elmer TGA instrument at a temperature ramp rate of 15 °C/min.

Finally, nitrogen sorption experiments were conducted for the pore analysis (volumes and sizes). The TriStar II 3020 micromeritics instrument was used and Joyner and Halenda (BJH), the most common method of deriving the pore size distribution from an appropriate nitrogen isotherm, was applied for the quantitative evaluation of the pore size distribution.⁴² Typical amounts of 0.0490 g Fe-NDC-M and 0.0321 g Fe-NDC-O were pre-desolvated at 250 °C for 18 h. Then, the samples were introduced into the N_2 gas sorption instrument at 77.35 K.

3. RESULTS AND DISCUSSION

3.1. XRD Patterns

Figure 5 represents the XRD patterns of Fe-NDC-M and Fe-NDC-O. The sharp peaks confirmed that the synthesized MOFs have crystalline structures. On the other hand, the angles of the sharp diffraction peaks ($2\theta = 7.5, 10, 10.5, \text{ and } 15^\circ$), for the two MOFs, are almost similar, indicating that their crystal sizes are in the same range.

3.2. SEM Results

Figure 6 depicts the SEM images of the MOFs. There were no differences in the size and shape of both samples. Most of the Fe-NDC-M/O nanoparticles seemed to have a rod-like shape with a diameter ranging between 50–80 nm and a length of 300–450 nm. However, few particles had larger sizes and their length reached approximately 600 nm. There were no differences between the external structure of Fe-NDC-M and Fe-NDC-O.

3.3. EDS Results

The analysis patterns at two different positions of the same sample for Fe-NDC-M and Fe-NDC-O are shown in Figures 7–10, respectively. A small amount of aluminum is present in the elemental analysis of Fe-NDC-M at the first

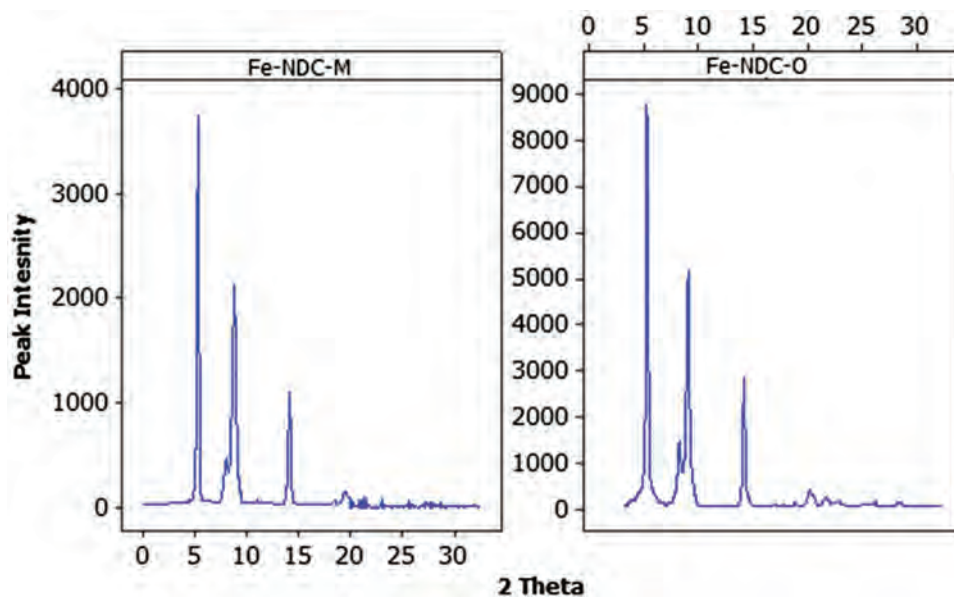


Figure 5. The XRD patterns of Fe-NDC-M (left) and Fe-NDC-O (right).

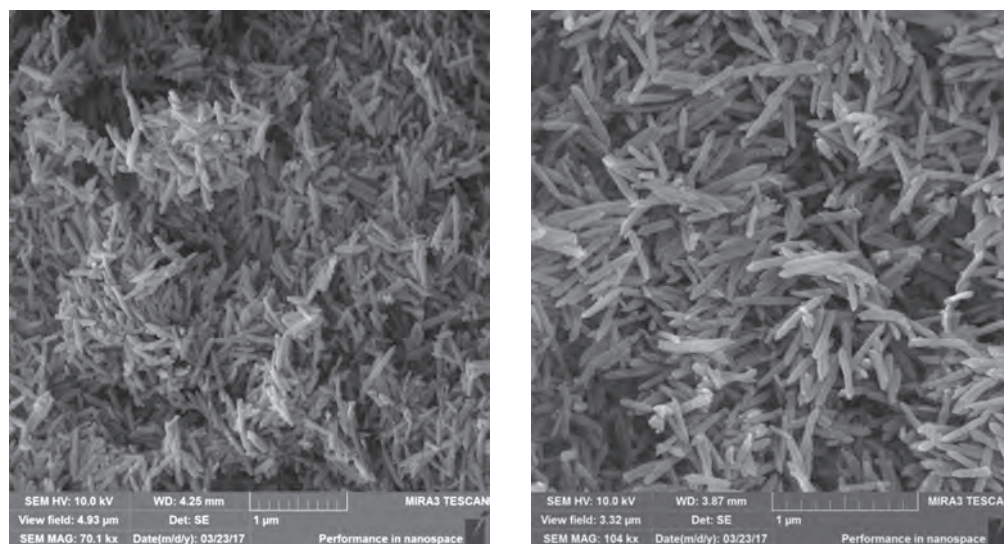


Figure 6. SEM images of Fe-NDC-M (left) and Fe-NDC-O (right).

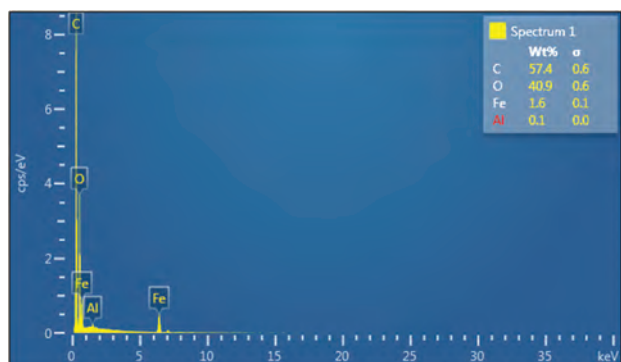


Figure 7. The elemental analysis of Fe-NDC-M at the first position.

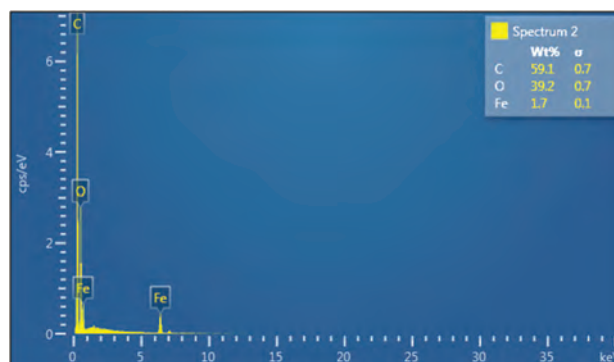


Figure 8. The elemental analysis of Fe-NDC-M at the second position.

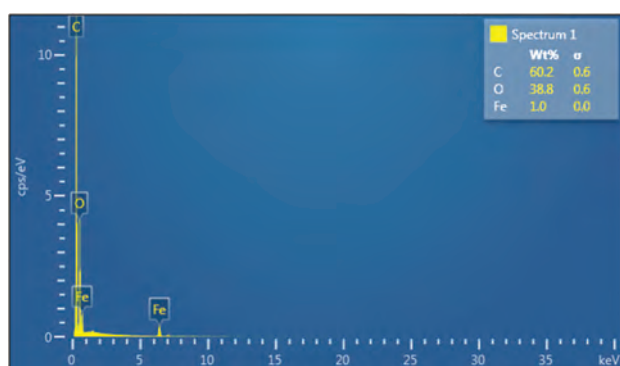


Figure 9. The elemental analysis of Fe-NDC-O at the first position.

position (from the aluminum stub on which the sample was placed). The difference between the composition wt.% at the two positions was minimal, which confirms the successful synthesis of both MOFs as well as the preparation reproducibility.

3.4. FTIR Spectra

The FTIR results showed that the absorption peaks of both MOFs were identical, which means that the stretching and bending of the covalent bonds in molecules were similar in Fe-NDC-M and Fe-NDC-O. By examining the overall spectrum, it can be seen that the number of the main characteristic absorption bands is greater than five. This assigns the samples as high-molecular-weight compounds. The two broad absorption bands at 3422.63 and 3421.95 cm^{-1} in the spectra, indicate the presence of a hydroxy group (H-bonded OH stretch), which originates from the organic linker (2,6-NDC). The band at 1655.11 cm^{-1} corresponds to a C=O group (carbonyl compound), that is found in 2,6-NDC. On the other hand, the absorption bands at 1605.47, 1606.28, 1571.25 and 1577.22, and 1496.47 cm^{-1} , which exist in the region 1615–1495 cm^{-1} , correspond to the presence of an aromatic compound (2,6-NDC). Additionally, the medium-to-strong absorptions at 797.77, 797.97, 770.86, and 771.37 cm^{-1} can also be used to support the presence of an aromatic structure

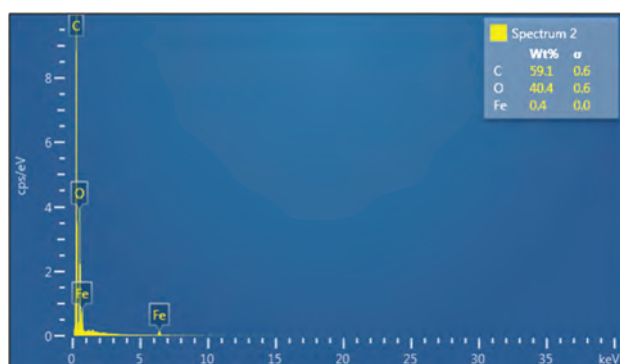


Figure 10. The elemental analysis of Fe-NDC-O at the second position.

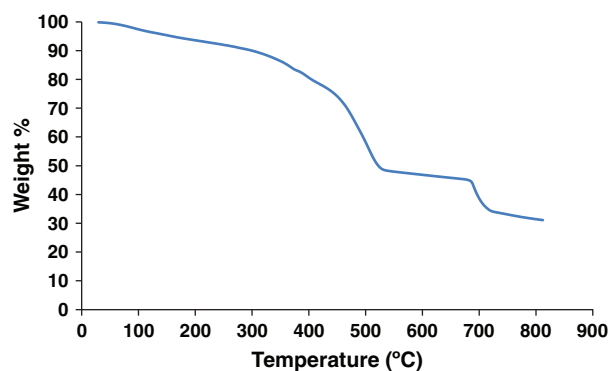


Figure 11. The TGA plot of Fe-NDC-M.

with a C–H out-of-plane bending on the aromatic ring. Additionally, the two peaks at 1103.90 and 924.65 cm^{-1} can be assigned to the in-plane C–H bending vibrations, which normally occur in the region 1150–950 cm^{-1} for aromatic compounds. Finally, all of the remaining absorption peaks (below 1700 cm^{-1}) confirm the presence of a carboxylic acid salt (2,6-NDC).⁴³

3.5. TGA Results

By examining Figures 11 and 12, it can be seen that the weight loss increased with increasing temperature over two consecutive steps. The first weight loss when comparing samples at room temperature and 300 °C (close to 10 and 15 wt. loss% of Fe-NDC-M and Fe-NDC-O, respectively) can be attributed to the removal of moisture and *N,N*-DMF molecules from within the pores of the material. More significant and pronounced decomposition appeared between 300–522 °C and 300–507 °C for Fe-NDC-M and Fe-NDC-O, respectively, where the samples weight loss reached to approximately 50 wt.% of their initial mass. This can be assigned to the thermal degradation of the structurally coordinated 2,6-NDC ligands. The other weight loss was observed between 687–727 °C and 694–721 °C for Fe-NDC-M and Fe-NDC-O, respectively, where the remaining samples weights at the end of this step were 34 and 31 wt.%. This loss is most probably due to

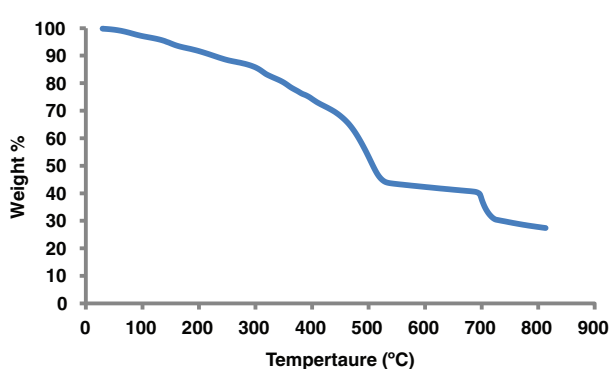


Figure 12. The TGA plot of Fe-NDC-O.

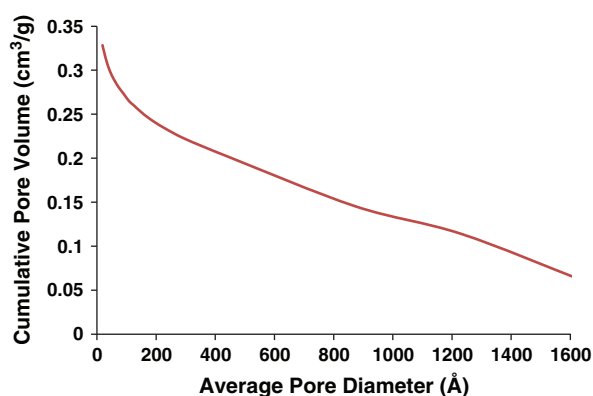


Figure 13. The BJH adsorption cumulative pore volume of Fe-NDC-M.

the decomposition of the metal ion (Fe^{+3}) from the MOF structure. The study concluded that both Fe-NDC-MOFs are thermally stable and the difference between their stability is insignificant.

3.6. N_2 Sorption Experiments at 77.35 K

BJH Adsorption pore distribution graphs are shown in Figures 13 and 14. Pore volumes and sizes results are summarized below.

Pore analysis of Fe-NDC-M:

- Single point adsorption total pore volume of pores less than 768.567 Å diameter at $p/p^\circ = 0.974153842:0.188083 \text{ cm}^3/\text{g}$.
- BJH Adsorption cumulative volume of pores between 17.000 Å and 3000.000 Å diameter: $0.328382 \text{ cm}^3/\text{g}$.
- BJH Adsorption average pore diameter: 148.551 Å.

Pore analysis of Fe-NDC-O:

- Single point adsorption total pore volume of pores less than 662.895 Å diameter at $p/p^\circ = 0.969927658:0.127138 \text{ cm}^3/\text{g}$.
- BJH Adsorption cumulative volume of pores between 17.000 Å and 3000.000 Å diameter: $0.255855 \text{ cm}^3/\text{g}$.
- BJH Adsorption average pore diameter: 139.265 Å.

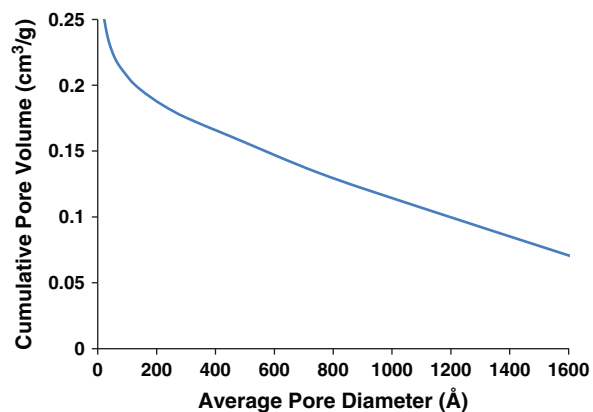


Figure 14. The BJH adsorption cumulative pore volume of Fe-NDC-O.

4. CONCLUSION

In conclusion, this study reports the successful synthesis of a novel MOF by combining iron nitrate with 2,6-naphthalenedicarboxylic acid in the presence of *N,N*-dimethylformamide via conventional solvothermal and microwave-assisted syntheses. The resulting pale yellow crystals were nanorods with diameters ranging between 50–80 nm and a length of 300–450 nm. The MOFs were found to have different covalent bonds between the molecules including: H-bonded OH stretch, C=O group, and C–H out-of-plane bending on the aromatic ring. Fe-MDC-MOF preparation steps are reproducible, and the particles were found to be thermally stable. The BJH adsorption average pore diameters were 148.551 Å and 139.265 Å for the Fe-NDC-M and Fe-NDC-O, respectively. The shape, size, and porosity of the highly crystalline designed MOFs render them suitable for drug delivery applications (especially for anticancer drug delivery systems). They can be used directly or functionalized by conjugating different targeting moieties to their surfaces.

Acknowledgments: The authors would like to acknowledge the support received from the American University of Sharjah Faculty Research Grants (AUS/FRG15-R-41 and AUS/FRG16-R-24); Patient's Friends Committee, Sharjah; AlJalila Foundation (AJF201555); and Al Qasimi Foundation.

References and Notes

1. L. R. MacGillivray, *Metal-Organic Frameworks: Design and Application*, John Wiley & Sons, Inc., New Jersey (2010).
2. P. Cheng, *Lanthanide Metal-Organic Frameworks*, Springer, Berlin, Heidelberg, Tianjin (2015).
3. R. J. Kupplera, D. J. Timmons, Q.-R. Fang, J.-R. Li, T. A. Makal, M. D. Young, D. Yuan, D. Zhao, W. Zhuang, and H.-C. Zhou, *Coord. Chem. Rev.* 253, 3042 (2009).
4. M. J. Rosseinsky, *Micropor. Mesopor. Mat.* 73, 15 (2004).
5. S. Keskin and S. Kızılal, *Ind. Eng. Chem. Res.* 50, 1799 (2011).
6. H. Furukawa, K. E. Cordova, M. O'Keeffe, and O. M. Yaghi, *AAAS* 341, 974 (2013).
7. C. Dey, T. Kundu, B. P. Biswal, A. Mallick, and R. Banerjee, *Acta Crystallogr. Sect. B* 70, 3 (2013).
8. F. Israr, D. K. Kim, Y. Kim, and W. Chun, *Química Nova* 39, 669 (2016).
9. Y. Cui, B. Li, H. He, W. Zhou, B. Chen, and G. Qian, *Acc. Chem. Res.* 49, 483 (2016).
10. Y.-R. Lee, J. Kim, and W.-S. Ahn, *Korean J. Chem. Eng.* 30, 1667 (2013).
11. Y. Zhao, K. Li, and J. Li, *Z. Naturforsch.* 65b, 976 (2010).
12. M. Alhamami, H. Doan, and C.-H. Cheng, *Materials* 7, 3198 (2004).
13. A. G. Marquez, A. Demessence, A. E. Platero-Prats, D. Heurtaux, P. Horcajada, C. Serre, J.-S. Chang, G. Férey, A. V. de la Peña-O'Shea, C. Boissiere, D. Grosso, and C. Sanchez, *Eur. J. Inorg. Chem.* 2012, 5165 (2012).
14. S. Qiu and G. Zhu, *Coord. Chem. Rev.* 253, 2891 (2009).
15. Y. Sun and H.-C. Zhou, *Sci. Tech. Adv. Mater.* 16, 1 (2015).
16. N. Stock and S. Biswas, *Chem. Rev.* 112, 933 (2012).
17. Z. Ni and R. I. Masel, *J. Am. Chem. Soc.* 128, 12394 (2006).
18. E. D. Dikio and A. M. Farah, *Chem. Sci. Trans.* 2, 1386 (2013).

19. M. Schröder, *Functional Metal-Organic Frameworks: Gas Storage, Separation and Catalysis*, Springer-Verlag, Berlin, Heidelberg, Nottingham (2010).
20. S. Ma and H.-C. Zhou, *Chem. Commun.* 46, 44 (2010).
21. B. Li, H.-M. Wen, W. Zhou, and B. Chen, *J. Phys. Chem. Lett.* 4, 3468 (2014).
22. V. I. Isaeva and L. M. Kustov, *Petrol. Chem.* 50, 167 (2010).
23. S. E. Miller, M. H. Teplensky, P. Z. Moghadam, and D. Fairen-Jimenez, *Interface Focus* 6, 1 (2016).
24. B. Li, M. Chrzanowski, Y. Zhang, and S. Ma, *Coord. Chem. Rev.* 307, 106 (2016).
25. P. Horcajada, R. Gref, T. Baati, P. K. Allan, G. Maurin, P. Couvreur, G. Férey, R. E. Morris, and C. Serre, *Chem. Rev.* 112, 1232 (2012).
26. R. C. Huxford, J. D. Rocca, and W. Lin, *Curr. Opin. Chem. Biol.* 14, 262 (2010).
27. A. C. McKinlay, R. E. Morris, P. Horcajada, G. Férey, R. Gref, P. Couvreur, and C. Serre, *Angew. Chem. Int. Ed.* 49, 6260 (2010).
28. P. Horcajada, T. Chalati, C. Serre, B. Gillet, C. Sebr, T. Baati, J. F. Eubank, D. Heurtaux, C. Clayette, C. Kreuz, J.-S. Chang, Y. K. Hwang, V. Marsaud, P.-N. Bories, L. Cynober, S. Gil, G. Férey, P. Couvreur, and R. Gref, *Nat. Mater.* 9, 172 (2010).
29. R. Liu, T. Yu, Z. Shi, and Z. Wang, *Int. J. Nanomedicine* 11, 1187 (2016).
30. K. M. L. Taylor-Pashow, J. D. Rocca, Z. Xie, S. Tran, and W. Lin, *ACS* 131, 14261 (2009).
31. J. Zhuang, C.-H. Kuo, L.-Y. Chou, D.-Y. Liu, E. Weerapana, and C.-K. Tsung, *ACS Nano* 8, 2812 (2014).
32. L.-L. Tan, H. Li, Y.-C. Qiu, D.-X. Chen, X. Wang, R.-Y. Pan, Y. Wang, S. X.-A. Zhang, B. Wang, and Y.-W. Yang, *Chem. Sci.* 6, 1640 (2015).
33. L.-L. Tan, H. Li, Y. Zhou, Y. Zhang, X. Feng, B. Wang, and Y.-W. Yang, *Small* 11, 3807 (2015).
34. L.-L. Tan, N. Song, S. X.-A. Zhang, H. Li, B. Wang, and Y.-W. Yang, *J. Mater. Chem. B* 4, 135 (2016).
35. H. R. Mooni, N. Kobayashi, and M. P. Suh, *Inorg. Chem.* 45, 8672 (2006).
36. D. Banerjee, S. J. Kim, and J. B. Paris, *Cryst. Growth Des.* 9, 2500 (2009).
37. A. Blomqvist, C. M. Araújo, P. Srepusharawoot, and R. Ahuja, *PNAS* 104, 20173 (2007).
38. I. Senkowska, F. Hoffmann, M. Fröba, J. Getzschmann, W. Böhlmann, and S. Kaskel, *Micropor. Mesopor. Mat.* 122, 93 (2009).
39. K. K. Gangu, S. Maddila, S. B. Mukkamala, and S. B. Jonnalagadda, *Ind. Eng. Chem. Res.* 56, 2917 (2017).
40. I. Bertini, *Bioinorganic Chemistry*, University Science Books, Mill Valley (1994).
41. D. E. Newbury and N. W. M. Ritchie, *J. Mater. Sci.* 50, 493 (2015).
42. K. Sing, *Colloids Surf., A* 187–188, 3 (2001).
43. J. Coates, *Interpretation of infrared spectra, a practical approach*, *Encyclopedia of Analytical Chemistry*, John Wiley & Sons Ltd., Newtown (2006), p. 10815.

Received: 15 July 2017. Accepted: 13 October 2017.